PARSIMONIOUS 3D PRESTACK KIRCHHOFF DEPTH MIGRATION

BIAOLONG HUA and GEORGE A. MCMECHAN

Center for Lithospheric Studies, The University of Texas at Dallas, 800 W. Campbell Road, Richardson, TX 75080-3021, U.S.A.

(Received September 10, 2008; accepted December 13, 2008)

ABSTRACT

Hua, B. and McMechan, G.A., 2009. Parsimonious 3D prestack Kirchhoff depth migration. *Journal of Seismic Exploration*, 18: 157-179.

A very fast 3D prestack Kirchhoff depth migration algorithm is developed. The computational cost is significantly reduced by six features. First, ray parameter information for the incident wave directions at the receiver locations is measured from input 3D seismic data in common source gathers and is used to reduce the amount of ray tracing required. Second, ray angles are binned and the ray corresponding to an angle bin is computed only once, regardless of how many times it occurs on a seismic trace. Third, the ray parameter file structure is optimized to eliminate redundancy associated with the overlap of seismic traces sharing the same receiver location. Fourth, fast two-point ray tracing is used to find the stationary reflection point on the receiver ray path that satisfies the time imaging condition.Fifth, the migration impulse response operator is reduced to the first Fresnel zone around the estimated stationary reflection point, which is much smaller than the large isochronic surface within the migration aperture in traditional Kirchhoff migration. Sixth, an amplitude threshold value is applied to decimate the input seismic data volume. The first four factors obviate the traditional traveltime table calculation before migration. Traveltime computation is embedded into the migration in the new algorithm. 3D synthetic prestack data test examples show that the new algorithm is two to three orders of magnitude faster than the traditional prestack Kirchhoff depth migration. The parsimonious images are cleaner than those obtained by traditional Kirchhoff migration, but are slightly less coherent.

KEY WORDS: migration, 3D imaging, Kirchhoff.

0963-0651/09/$5.00

INTRODUCTION

3D poststack migration has been routinely applied in seismic data processing. The basic assumption of 3D poststack migration is that the conventionally stacked seismic data volume is a good approximation of zero-offset data. This assumption is valid only when the lateral velocity variations are locally weak so reflection times are hyperbolic. If there are reflections with conflicting dips (and hence have different stacking velocities), the conventionally stacked data volume will no longer be a good approximation to a zero-offset volume. Migration after stack is not suitable for accurately imaging complex subsurface structures; prestack migration is needed. Kirchhoff migration has the advantages in 3D that it can be used to process arbitrary subsets of the input seismic data, to image complex geological structures with steep dips [even turned waves (Ratcliff et al., 1992; Ratcliff et al., 1994)], and it can accommodate irregular acquisition geometries. However, the high computational cost of 3D prestack Kirchhoff depth migration is still detrimental to routine application.

Prestack depth migration is sensitive to the input migration velocity. Conventional velocity estimation methods (stacking velocity analysis, velocity spectra, time migration velocity analysis) have difficulties in accommodating lateral velocity variations. An accurate migration velocity field must be iteratively estimated and re-estimated using the migration procedure itself. Thus, a fast 3D migration algorithm becomes the dominant component in the estimation of velocity by iterative migration (Fei and McMechan, 2006a,b).

The purpose of this paper is to present a new input-based 3D prestack Kirchhoff-type depth migration algorithm which is very fast, and efficient in its use of memory and disk-space. The new algorithm can be run on workstations, not only on supercomputers or processor clusters, can be used in 3D fast iterative migration velocity analysis, and even in real-time migration imaging for quality control in the field.

The 3D prestack parsimonious depth migration is the last in a series of parsimonious migration algorithms developed by Hua and McMechan (1999, 2001, 2003, 2005). For one reflection on one trace, the ray parameter is estimated at the receiver location in the common source gather and a single ray is traced back into the velocity model from the receiver location. Then a fast two-point ray tracing technique (Um and Thurber, 1987) finds the stationary reflection point which satisfies the time image condition. The sample amplitude is imaged over the first Fresnel zone of the local reflector surface around the stationary reflection point.

In the methodology section, we describe the algorithm and the implementation of parsimonious 3D prestack Kirchhoff depth migration. In the Numerical Examples section, two synthetic 3D prestack data sets are used to test the feasibility of the new method. An analysis of the computational efficiency of parsimonious migration is given in the Discussion section.

METHOD

3D prestack parsimonious depth migration has three main steps: (1) estimation of ray parameters at the receiver locations; (2) an optional re-arrangement of the ray parameter file structure; and (3) imaging of sample amplitudes. The following three subsections detail each of these three steps in turn.

Estimation of ray parameters at receiver locations

The details of the ray parameter estimation in 3D parsimonious migration depend on the acquisition geometry. 3D survey geometries can be quite different depending on the structure of interest. A common feature through the many different types of acquisition layouts, such as swath geometry, orthogonal geometry and button patch etc. (Cordsen et al., 2000) is that the source interval is usually much larger than the receiver interval. Thus, estimation of ray parameters by a local 3D slant stack is expected to be viable for samples on each trace only at the receiver location for most 3D acquisition geometries.

We assume a swath acquisition geometry (Fig. 1) (Cordsen et al., 2000), in which each seismic source is recorded on a number of parallel cables. Suppose there are enough cables (at least five, but preferably many more) associated with each source so that a wavefront orientation can be defined in 3D and the cable interval and the geophone interval on each cable are small enough that the data are not spatially aliased. Then, we can estimate ray parameters for the peak/trough samples on each trace at the receiver location in common-source gathers by local slant stacking (Hua, 2003).

An amplitude threshold is applied to each seismic trace, after time-dependent scaling; only the peak and trough sample points on each trace whose relative amplitude is greater than a predefined amplitude threshold are used for estimation of ray parameters (Hua and McMechan, 1999, 2001, 2003, 2005; Hua, 2002). Thus, the amount of input data used for migration is limited to the most salient features and is thereby reduced greatly and the migration speed is corresponding improved.

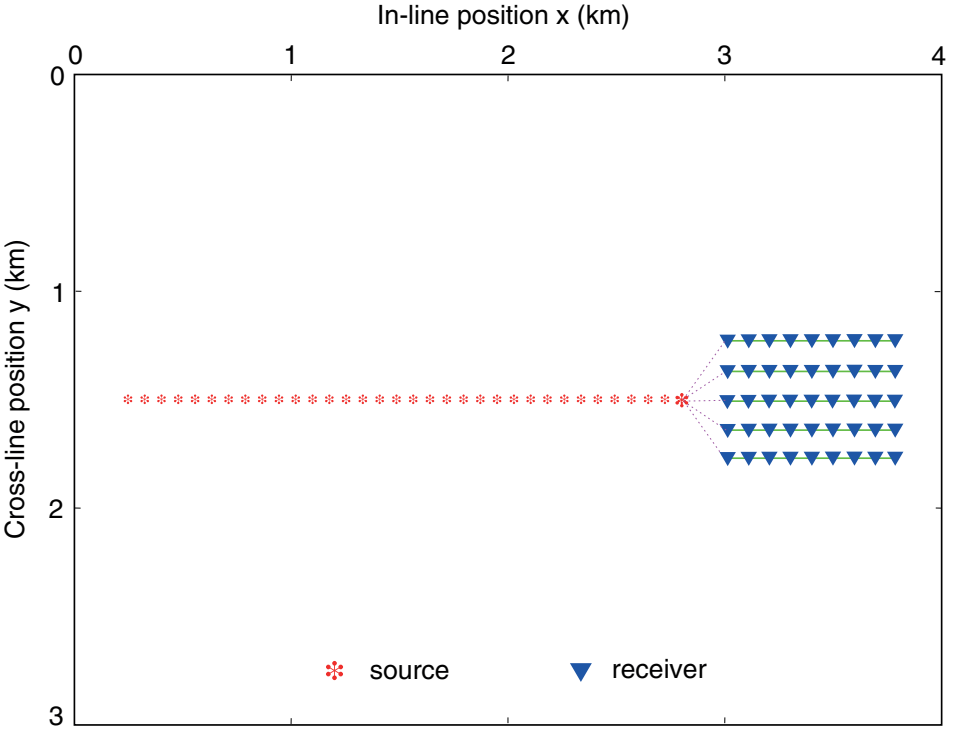

Fig. 1. Acquisition geometry. Seismic data are acquired in common-source gathers. Each source is associated with many parallel receiver lines, and each receiver line has many geophones. The receiver lines and the geophones for each source are uniformly distributed. For the three-layer model in Fig. 3, there are 34 sources, along a straight line at y = 1.5 km on the surface in the in-line direction with a source interval of 0.08 km. Each source is recorded on 61 parallel receiver lines with a line interval of 0.01 km; each receiver line has 81 receivers with a receiver interval of 0.01 km. The minimum in-line source-receiver offset is 0.2 km and the maximum in-line offset is 1.0 km.

The ray parameter estimation for each trace is done in two perpendicular directions (usually the in-line and cross-line directions). The final horizontal ray parameter for each reflection is given by the vector combination of its two orthogonal apparent ray parameter components. Equivalently, one could fit a plane through the reflection on a group of adjacent traces, regardless of their directions from the central trace. The amount of data in the crossline direction is typically much less than in the inline direction, so the crossline p-values are correspondingly less reliable. However, current Ramform ship configurations (Coffin et al., 1998; Petroleum Geo-Services, 2008) provide up to 20 hydrophone streamers with separation up to 150 meters, which should be sufficient (and a two ship recording configuration could have 40 streamers!).

For land data, apertures can be designed to satisfy any requirements (within the budget) and so do not have a technical limitation. Wave incident directions can also be measured from three component land or VSP data via polarization analysis (e.g., Agnihotri and McMechan, 2007). So, there are a number of situations in which adequate data for parsimonious migration are potentially available. A 2D field data example is shown by Hua and McMechan (2001).

Ray parameter file reorganization

The estimated ray parameters for each trace at the receiver locations may be (optionally) rearranged and grouped by the location of the trace, to eliminate the p-value redundancy in each common receiver gather (Hua and McMechan, 2003). The efficiency gain from the rearrangement of the ray parameter file structure depends on the total fold of the survey geometry, which equals the product of the in-line fold and the cross-line fold (Cordsen et al., 2000). The larger the total fold, the greater the efficiency gain. The total fold for the two test examples in next section is about 10, and the migration speed has been doubled by the rearrangement of the ray parameter file structure. If the total fold is 30, the efficiency gain from ray parameter file reorganization would be at least 6.

We do not estimate ray parameters for samples on each trace at the source location, since the source locations may be irregular and the source interval may be too large for reliable p-value estimation.This would also involve sorting the data into common-receiver gathers, which would be an added expense and would require additional disk-space.

Imaging of sample amplitudes

Let the two estimated apparent ray parameters from the first step (above) at receiver location R for a peak/trough sample point on a seismic trace be p_x in the x-direction and p_y in the y-direction. The migration of a peak/trough sample on the seismic trace is performed as follows:

1. Evaluate the ray azimuth and incident angles (φ and θ) at the receiver location (Fig. 2) using

$$1/v^2 = p_x^2 + p_y^2 + p_z^2 \quad , \tag{1a}$$

$$\tan\varphi = p_y/p_x \quad , \tag{1b}$$

and

$$\tan\theta = [\sqrt{(p_x^2 + p_y^2)}]/p_z \quad . \tag{1c}$$

Here, v is the propagation velocity in the near surface, and p_z is the apparent ray parameter in the vertical direction. v can be obtained from first breaks for land data, and is the water velocity for marine data.

2. Shoot a ray from the receiver location with the azimuth angle φ and incident angle θ, up to some maximum time which is greater than half the arrival time and is dip-dependent. We use an adaptive stepsize Runge-Kutta method (Press et al., 1992) to solve the 3D kinematic shooting ray tracing equations (Červený et al., 1977).

3. Find the point P on the receiver ray path where the time imaging condition

$$t_s + t_r = t_a \quad , \tag{2}$$

is satisfied, where t_s is the traveltime of the ray path from the source location S to point P, t_r is the traveltime of the ray path from the point P to the receiver location R, and t_a is the observed arrival time of the time sample. Point P will be the stationary reflection point for the time sample. We use the fast two-point ray tracing algorithm by Um and Thurber (1987), in which the ray tracing equations are replaced by simple algebraic operations, to iterate to locate the position of point P.

The procedure of determining the position of reflection point P on the receiver ray path is (Fig. 2):

a. Pick the point on the receiver ray path whose traveltime is half the arrival time t_a of the time sample. Denote this time as t_r.

b. Compute the traveltime t_s of the ray path from the source location to the point picked in (a) by two-point ray tracing.

c. Compute the sum t_c of the calculated traveltimes t_s from step (b) and t_r from step (a); $t_c = t_s + t_r$. Then, calculate the time difference $\Delta t = t_c - t_a$ between the calculated and the observed reflection times.

d. If the absolute time difference $|\Delta t|$ in step (c) is less than a predefined value (for example less than 0.001 s), then the point is taken as the required stationary reflection point, and go to step (4). If the time difference Δt in step (c) is less than zero, we pick a new point on the receiver ray path whose traveltime to the source point is estimated to be $t_s + \Delta t/2$; if Δt is greater than zero, we pick a new point on the receiver ray path whose traveltime to the source point is estimated to be $t_s - \Delta t/2$.

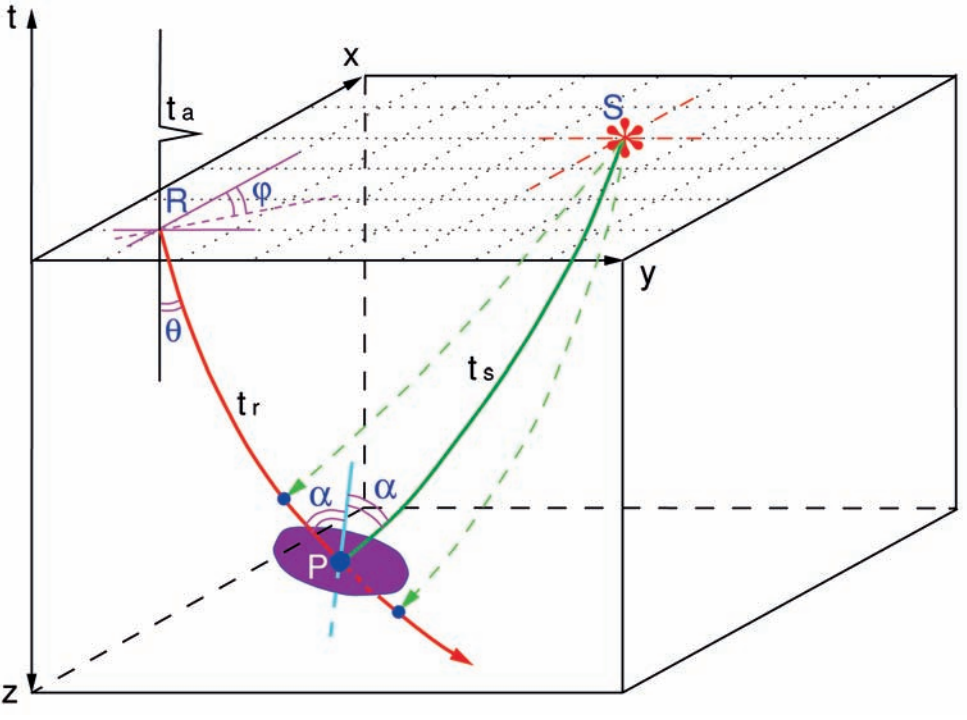

Fig. 2. Implementation of 3D prestack parsimonious Kirchhoff depth migration. A single ray (red) is traced from the receiver location R with the estimated azimuth angle φ and incident angle θ. φ is in the horizontal plane and θ is in the vertical plane. Then, a fast two-point ray tracing technique is used to trace the source ray (green) and to find the stationary reflection point along the receiver ray that satisfies the time imaging condition $t_a = t_s + t_r$. The amplitude of the time sample is inserted into the local image surface only within the first Fresnel zone (the purple patch).

e. Repeat steps (b), (c) and (d) to find the point on the receiver ray path that satisfies the convergence condition in step (d). The resulting point P satisfies the time imaging condition and is the stationary reflection point in the image space for the time sample. Usually, 2-3 iterations are sufficient.

4. Find the normal to the reflector by bisecting the angle (2α in Fig. 2) between the source and receiver rays. The orientation of the local reflector surface in the image space is perpendicular to the ray bisection vector in step (4), by Snell's law.

5. Define the location of the points on the local reflector surface at which the time sample is imaged. The region of the contribution to the reflector image is defined as the circular patch within the first Fresnel zone (Sheriff and Geldart 1982).

6. Add the amplitude of the time sample into the local reflector surface that was found in step (5). To reduce stack artifacts, the inserted amplitude is tapered to zero from the center to the edge of the Fresnel zone.

7. Repeat the above steps for all the time samples, that correspond to peaks and troughs above the amplitude threshold, to complete the migration.

NUMERICAL EXAMPLES

The proposed 3D parsimonious prestack Kirchhoff migration algorithm has been tested using two synthetic 3D prestack data sets for a three-layer model and for a subset of the SEG/EAGE salt body model (Aminzadeh et al., 1997). Each of these is presented in turn.

Three-layer model

The three-layer model (Figs. 3a and 3b) has two curved reflector surfaces, a shallow anticlinal surface and a deep synclinal surface. The model size is 4.0 $\times$ 3.0 $\times$ 2.0 km (in-line $\times$ cross-line $\times$ depth) and is discretized into 401 $\times$ 301 $\times$ 201 grid points with a grid increment of 0.01 km in all three dimensions.

An eighth order finite-difference implementation of the scalar wave equation (Fornberg, 1988) is used to synthesize 34 common-source gathers. Fig. 1 contains a cartoon of the survey geometry; to simulate a subset of a larger 3D survey, data for a single line of common-source gathers are calculated in the in-line direction at y = 1.5 km. The sources lie between x = 0.23 km and x = 2.87 km; the source increment in the in-line direction is 0.08 km. Each source has 61 parallel receiver lines centered on the source line, and the receiver line interval is 0.01 km. Each receiver line has 81 receivers with interval of 0.01 km. The smallest offset in the in-line direction is 0.2 km and the maximum offset in the in-line direction is 1.0 km. The total number of traces is 34 sources $\times$ 61 lines $\times$ 81 receivers = 167994. There are 451 sample points on each trace and the time sampling interval is 0.004 s. Figs. 4a and 4b contain slices through the representative common-source gather for the source at x = 1.03 km on the surface.

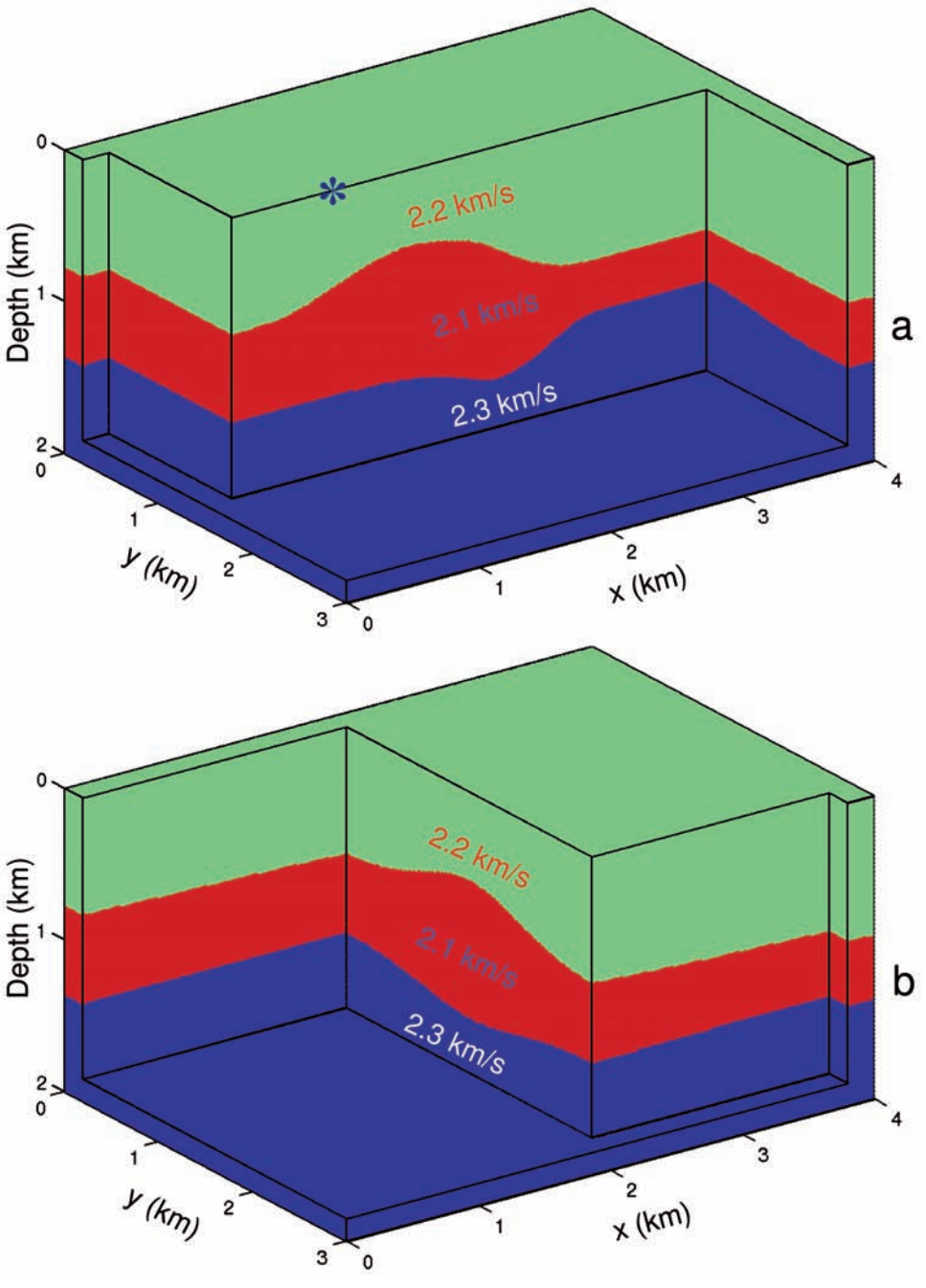

Fig. 3. Representative slices through the three-layer test velocity model. The star (*) in (a) is the location of the source for the common-source gather shown in Fig. 4.

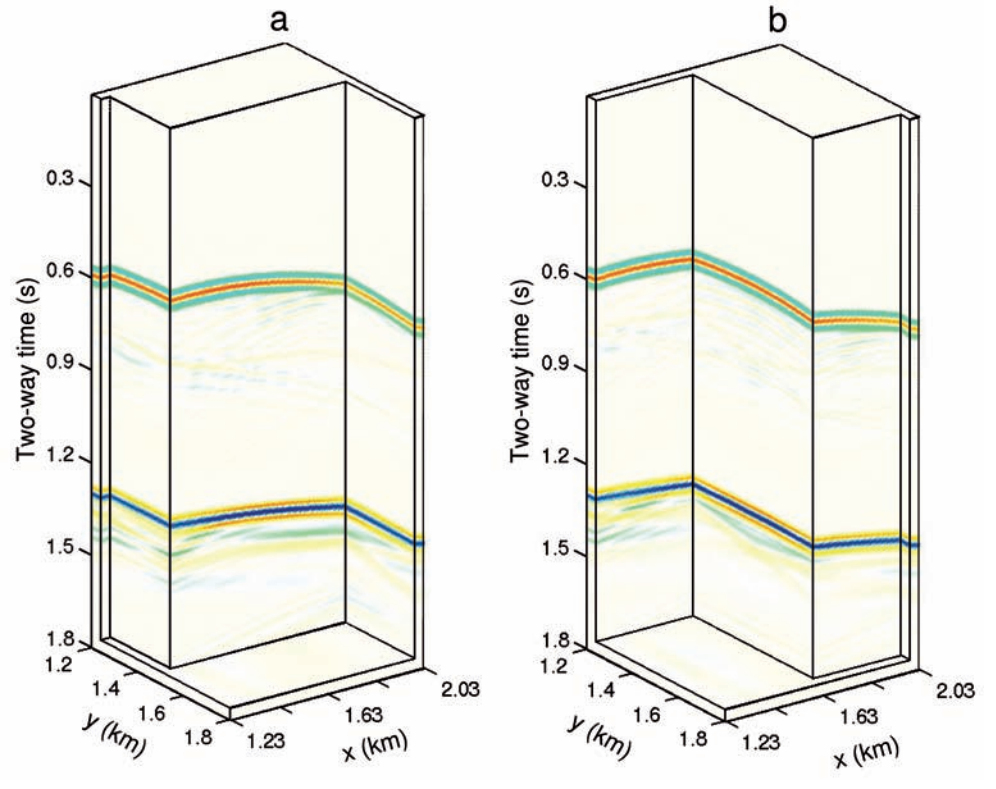

Fig. 4. Representative slices through the representative synthetic common-source gather for a source at x = 1.03 km on the surface of the three-layer model in Fig. 3 (at the star *). The direct wave has been removed.

Figs. 5a and 5b display the migration results for the 3D prestack parsimonious Kirchhoff depth migration for the single line of 34 sources. A smoothed version of the velocity model in Fig. 3 is used for migration. The grid increment in the migrated image is 0.01 km in all three dimensions. The structures in the in-line direction (Fig. 5a) are well imaged. Since there is only one source line in the data set, the image in the cross-line direction (Fig. 5b) is incomplete, but the portion of the structures that are illuminated are accurately imaged. Superimposing images from additional source lines would fill out the entire image volume.

The full 3D conventional implementation of prestack Kirchhoff depth migration is time-intensive and is almost impossible to complete on workstations in an affordable time (hours to days) even for this relatively small model. Thus, for comparison, we here migrate only selected target slices using the algorithm

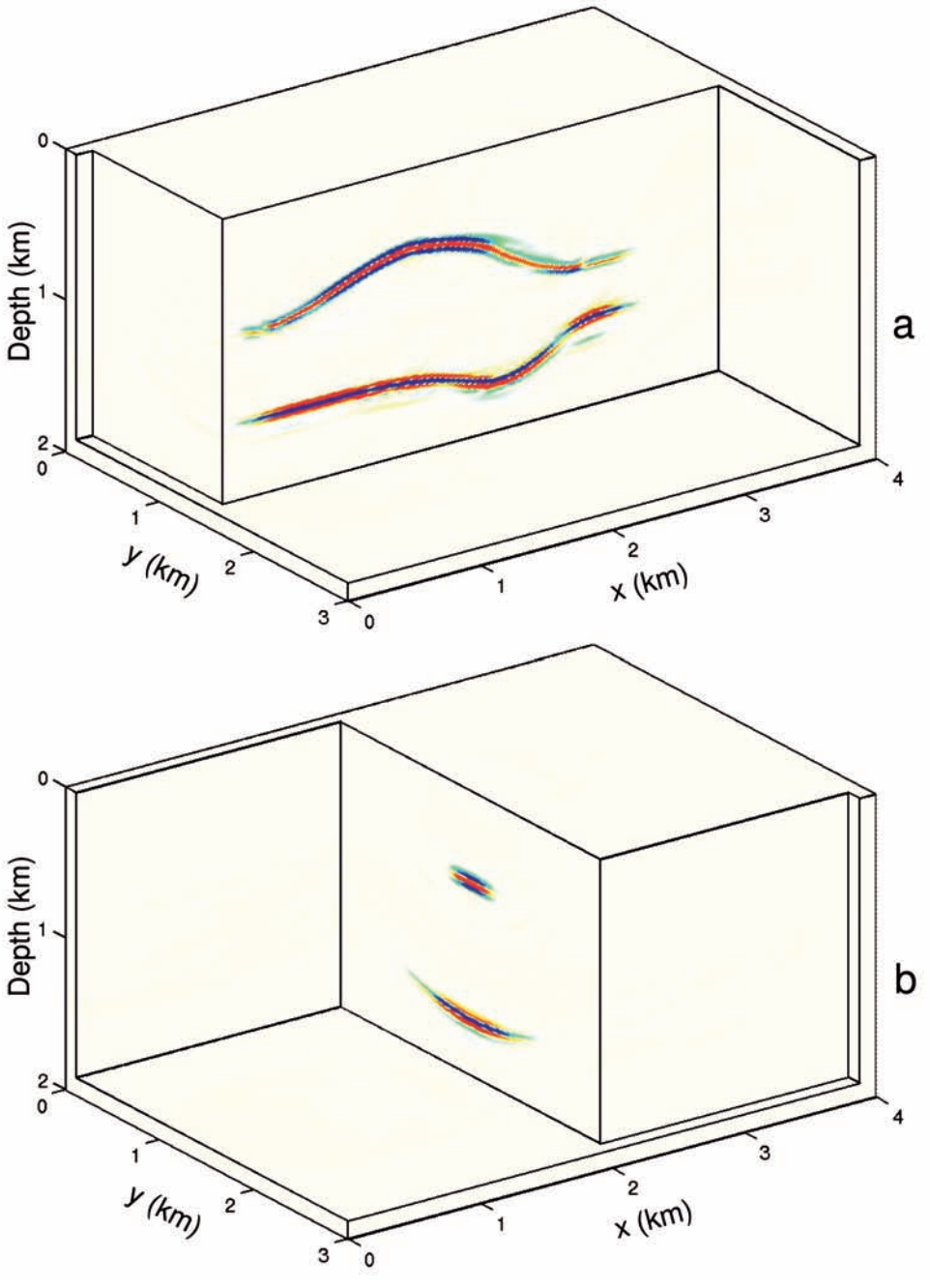

Fig. 5. 3D prestack parsimonious Kirchhoff depth migrated partial image for one line of 34 sources over the three-layer model. Panels (a) and (b) show the partial images on the same slices through the velocity model in Figs. 3a and 3b.

of Epili and McMechan (1996). The full migrated image can be obtained by migrating all the slices in the image cube (one-by-one, or in parallel in a cluster environment).

For the three-layer model, we select the middle profile beneath the source line (at y = 1.5 km) as the target slice for comparison with the 3D conventional migration [see the model section along the in-line (constant y) direction in Fig. 3a]. The migration grid increment of the target slice is 0.01 km in both the horizontal and vertical directions (the same as in the parsimonious migration). To reduce the requirements of disk-space for the traveltime tables, a coarse grid increment of 0.04 km in the horizontal and vertical directions on the slice is used for each traveltime table, and the source interval between traveltime tables in the in-line and cross-line direction on the surface is also 0.04 km. Traveltimes for the fine (0.01 km) migration grid points are interpolated between the coarse (0.04 km) grid points of the traveltime tables. A fast two-point ray tracer (Um and Thurber, 1987) is used to calculate the traveltime table.

The conventional 3D prestack slice Kirchhoff migration result for the target slice is shown in Fig. 6b, together with the 3D prestack parsimonious migration result (Fig. 6a). The parsimonious migration image looks quite clean compared with the conventional migration image. The reasons are: (1) the impulse response of parsimonious migration is confined to the first Fresnel zone, and so the image is free of the long-tail artifacts (caused by source aliasing) in conventional migration (labeled 1, 2, 3 and 4 in Fig. 6b); (2) application of the amplitude threshold in parsimonious migration removes some of the small amplitude noise (labeled 5 in Fig. 6b). Although the main features in both outputs are similar, the parsimonious migration is much faster than conventional migration; detailed analysis of the computation costs for the two algorithms is given in the Discussion section.

SEG/EAGE salt model

For the second example, an 8.0 × 3.0 × 2.0 km portion (Figs. 7a and 7b) is cut from the SEG/EAGE salt model (Aminzadeh et al., 1997). The model is discretized into 801 × 301 × 201 grid points with a grid increment of 0.01 km in all three directions. An eighth-order finite-difference solution of the scalar wave equation (Fornberg 1988) is used to synthesize one line of 29 common-source gathers. The survey geometry is similar to that used for the three-layer model (Fig. 1). The sources are along a survey line in the in-line direction in the middle of the model (y = 1.5 km). The in-line position of the first source is x = 0.2 km and the source increment in the in-line direction is 0.2 km. Each source has 101 parallel receiver lines centered on the source line,

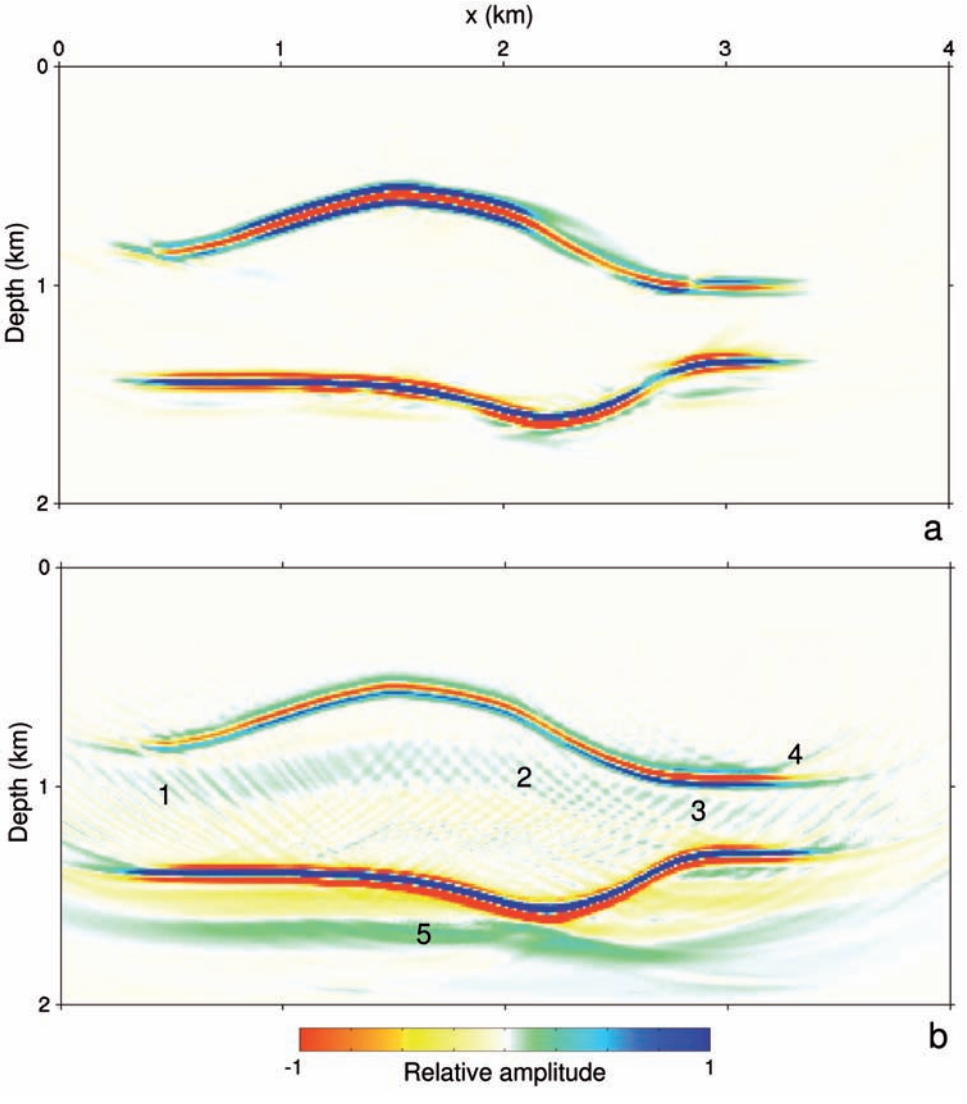

Fig. 6. Partial image migration results for the three-layer model. (a) is the parsimonious migration image. (b) is the conventional Kirchhoff migration image for the same slice as in (a). The images are partial because data from only one line of sources are used.

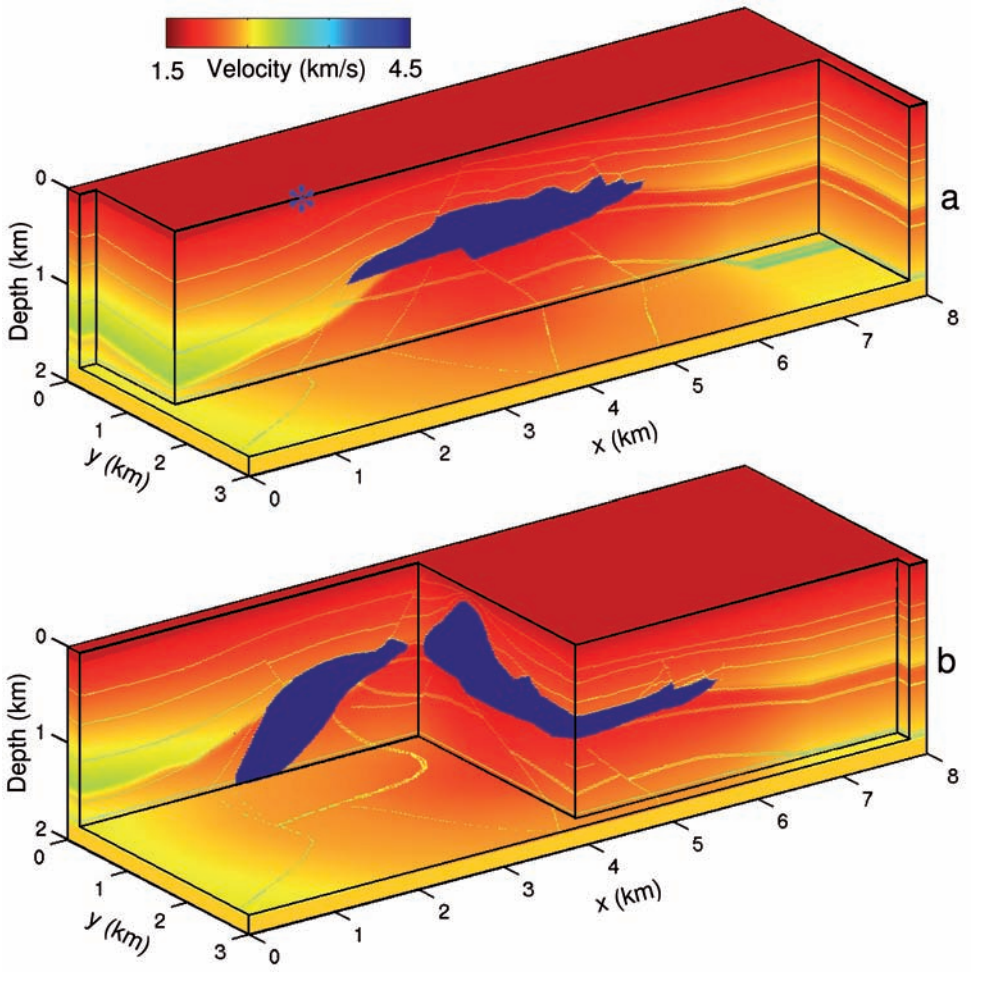

Fig. 7. Cut-away displays of the SEG/EAGE salt velocity model.The star (*) in (a) is the location of the source for the common-source gather shown in Fig. 8.

and receiver line interval is 0.01 km. Each receiver line has 201 receivers with interval of 0.01 km. The smallest offset in the in-line direction is 0.0 km and the maximum offset in the in-line direction is 2.0 km. The total number of traces is 29 sources $\times$ 101 lines $\times$ 201 receivers = 588729. There are 501 sample points on each trace and the time sampling interval is 0.004 s. Figs. 8a and 8b contain slices through the common-source data volume for the source at the in-line position of x = 2.0 km.

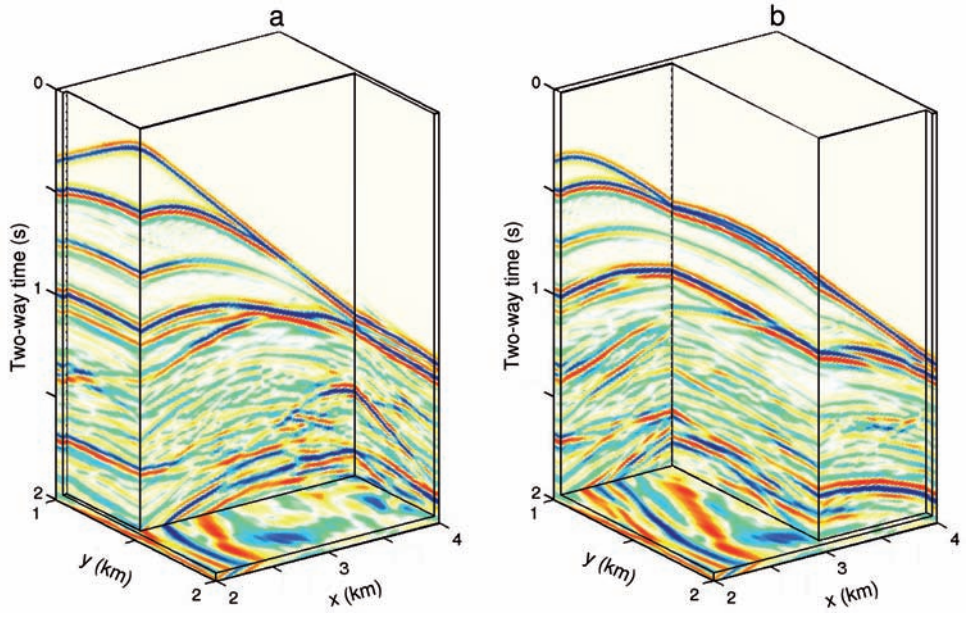

Fig. 8. Cut-away displays of a representative synthetic common-source data volume for the SEG/EAGE salt model for a source at the in-line position y = 2.0 km on the surface of the model in Fig. 7 (at the star *). The direct wave has been removed.

Figs. 9a and 9b contain cut-away displays of the migration results of the 3D prestack parsimonious Kirchhoff depth migration. The velocity model in Fig. 7 is smoothed for input to migration. The grid increment of the parsimonious migration image is 0.01 km in all three directions. In the parsimonious migration result in the in-line direction (Fig. 9a), the sedimentary reflectors are well reconstructed. The bottom of the salt body is well outlined, but the top is blurred because the geometry of the salt top in the cross-line direction is quite complicated (Fig. 7b), much of the energy reflected from the steep dips at the

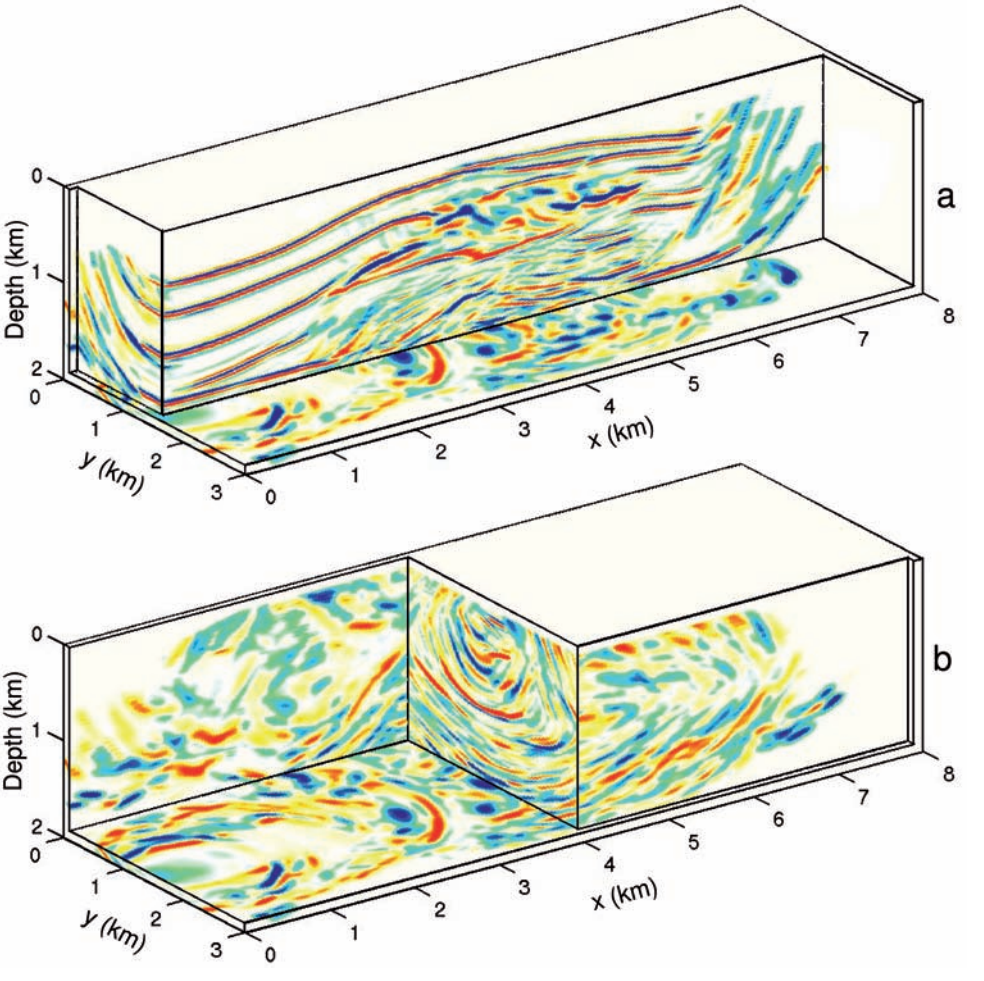

Fig. 9. Cut-away displays of 3D prestack parsimonious Kirchhoff depth migrated results of the salt model. The slice positions are the same as those shown in the velocity models in Figs. 7a and 7b. The image is partial because data from only one line of sources are used.

top of the salt body is out of the recorded survey aperture, and the source spacing (200 m) is aliased. The image deteriorates past x $\sim$ 6.5 km because that corresponds to the last survey midpoint. There are some upward curving migration artifacts at x $>$ 6 km caused by a few erroneous ray path directions. Some of the most steeply dipping parts of the structure are not imaged because of the partial illumination by the input data from the single survey line used.

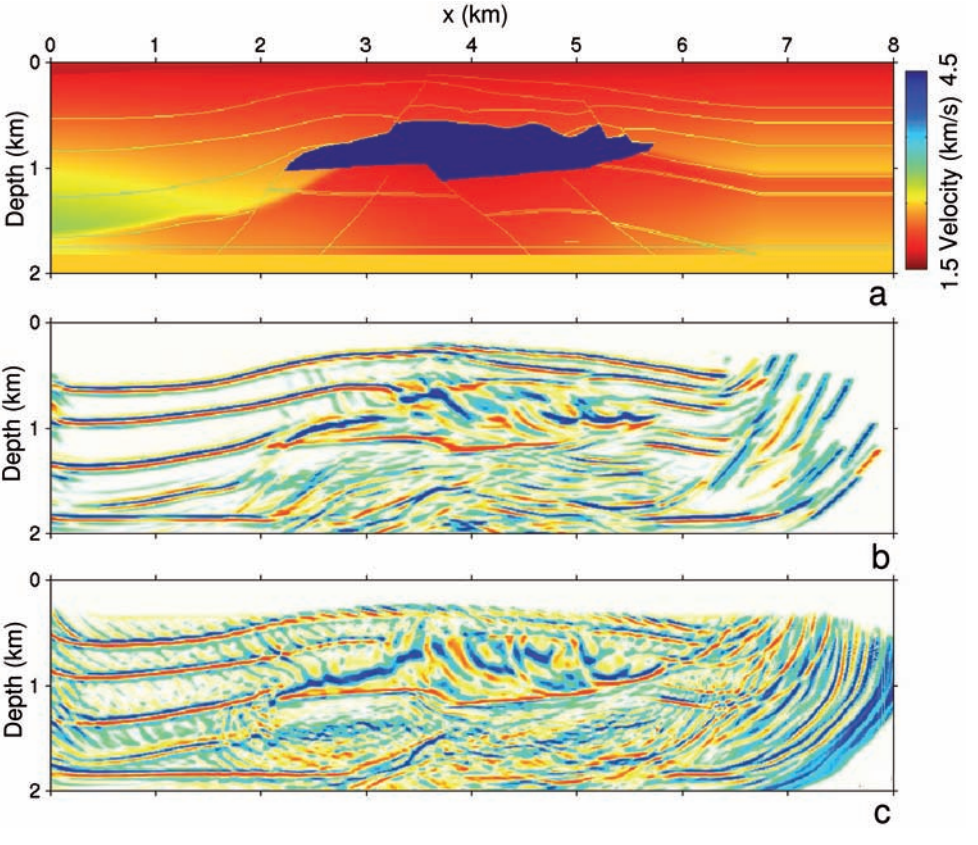

Fig. 10. Partial migration image results for the salt model. (a) is the velocity model slice corresponding to the migrated images. (b) is the parsimonious migrated image. (c) is the conventional Kirchhoff migrated image for the same slice as in (b). The images are partial because data from only one line of sources are used. Most of the artifacts in (c) are caused by aliasing of the sources.

For comparison, only one slice at y = 1.5 km (see Fig. 7a) is migrated using the conventional Kirchhoff migration. The grid increment of the migrated image on the target slice is 0.01 km in both the horizontal and vertical directions (the same as in the parsimonious migration). The grid increment for each traveltime table is 0.04 km both in the horizontal and vertical directions on the slice. The receiver interval between traveltime tables in the in-line and cross-line directions on the surface is also 0.04 km; source locations are coincident with some of the receivers. A fast two-point ray tracing technique (Um and Thurber, 1987) is used to calculate the traveltime tables. Traveltimes for the finer migration grid (0.01 km) points are interpolated from the coarse grid (0.04 km) points of the traveltime tables.

The image obtained by conventional 3D prestack Kirchhoff migration for the target slice is shown in Fig. 10c, together with the 3D prestack parsimonious migration result (Fig. 10b) and the vertical model slice (Fig. 10a) at the same location. The parsimonious migrated image (Fig. 10b) is comparable in information content to the conventional migrated image (Fig. 10c). The noise in the conventional migrated image comes partly from the background noise in the input data, and partly comes from the long-tail artifacts of the impulse response; the effect of the aliasing of the sources is much more visible in the conventional image than in the parsimonious image. Parsimonious migration is relatively free of such background noise because the application of the amplitude threshold which removes most of the small amplitude noise, and because of the small (one Fresnel zone) aperture of the impulse response. Neither conventional migration nor parsimonious migration can image the top of the salt body and the steep dip fault structures because of the limited illumination provided by the single line of sources in the input data. The salt surfaces should be better imaged and the artifacts further reduced in both the traditional and parsimonious migrations by adding data from more survey lines, parallel to the one used here, and by using unaliased sources.Given that they are both partial, the comparison of the parsimonious and conventional images confirms the viability of the parsimonious approach.

DISCUSSION

The current implementation of parsimonious migration focuses mainly on significantly improving the migration speed; preserving accurate amplitude is not an objective of parsimonious migration. The quality and completeness of parsimonious migration images is affected by the values chosen for the amplitude threshold, and for the p-increment [see Hua and McMechan (2003) for 2D examples]. The smaller the amplitude threshold, the more data are kept for migration input, and thus, the more structural information that is retained in the migrated image. The smaller the p-increment, the more accurate the estimated p-value and the subsequent incident ray path are, so the more

consistent the migration image is. The uncertainty in the input migration velocity will also affect parsimonious images in the same way as in conventional Kirchhoff migration. Image smiles result if the velocity is too high, and frowns result if the velocity is too low (Yilmaz, 2001). The near surface velocity is more important in parsimonious migration than in conventional migration because the calculation of the initial ray angles depends on the near surface velocity [see eq. (1a)]. The reader is referred to Hua and McMechan (2003) for a more detailed discussion on the factors that affect the migration quality, and the amplitude issues in parsimonious migration. The remainder of this section contains a comparison of computation costs for the conventional migration and the parsimonious migration, and then analyses the main factors contributing to the efficiency gains of parsimonious migration.

Comparison of computation costs

The computation times for conventional migration and parsimonious migration for the three-layer model and the salt model are listed in Table 1. The conventional implementation of full 3D prestack Kirchhoff depth migration is time intensive and requires a huge memory and diskspace for large 3D problems. In Table 1, the computation time for the conventional migration is for migration of only one slice of the 3D image, but the computation time for the parsimonious migration is for migration of the full 3D volume. If 50 slices are migrated by conventional slice Kirchhoff migration, then, for the three-layer model, the total computation time for conventional migration (Tc) is estimated to be 14577.0 minutes, while the total time for parsimonious migration (Tp) is

Table 1. Comparison of computation times for conventional Kirchhoff migration and parsimonious Kirchhoff migration. Tc is the total time for conventional migration, Tp is the total time for parsimonious migration, and Tm is the time for only migration in parsimonious migration. The migration grid increment for both the conventional and parsimonious migrations is 0.01 km. Traveltime grid increment for the conventional migration is 0.04 km. The computation times listed for the conventional migration are those for migrating only one slice of each of the two models, and the computation times for the parsimonious migration are for 3D prestack migration of the whole volumes. All computations are done using one Silicon Graphics Origin 2000 processor with 2 GB memory.

Model	Time for conventional migration (minutes)			Time for parsimonious migration (minutes)			Relative efficiency for 50 model slices	
	Ray tracing	Migration	Total (Tc)	p-value estimation	Migration (Tm)	Total (Tp)	$\frac{Tc(50)}{Tp}$	$\frac{Tc(50)}{Tm}$
3-Layer model	123.5	168.0	291.5	6.4	36.2	42.6	342.1	402.6
Salt model	2113.7	1095.6	3209.3	105.5	569.2	674.7	237.8	281.9

only 42.6 minutes, so the relative efficiency Tc/Tp of the parsimonious migration is ~ 342. For the salt model, the total computation time for conventional migration of 50 slices is estimated to be 160466.0 minutes, and the total time for parsimonious migration is about 674.6 minutes, so the parsimonious migration efficiency Tc/Tp is ~ 237. Table 1 also gives another measure of relative efficiency Tc/Tm, which is the total time of conventional migration for migration only relative to that in parsimonious migration. Tc/Tm makes sense because p-value estimation in parsimonious migration needs to be done only once no matter how many times migration is performed. Tc/Tm is ~ 403 for the three-layer model, and ~ 282 for the salt model. So, parsimonious 3D prestack Kirchhoff depth migration is significantly faster than conventional 3D prestack Kirchhoff depth migration. Thus, for any applications (such as migration velocity analysis) that include iterative migration, the parsimonious approach has significant advantages. Hua and McMechan (2003) demonstrate the potential of velocity estimation using 2D parsimonious migration, and Fei and McMechan (2006a,b) demonstrate feasibility in 2D and 3D, respectively.

Factors contributing to efficiency gains

The main factors contributing to the efficiency gains of parsimonious migration are:

1. The amount of ray tracing is greatly reduced because of the use of ray parameters measured from the input seismic data as *a priori* information. For example, assume that both the azimuth angle increment and incident angle increment are 2° and the maximum incident angle is 60°. Then, 181 × 30 = 5430 rays have to be traced from each source (or receiver) position in conventional migration. In the salt model example above, the maximum number of rays traced for each source (or receiver) position in parsimonious migration is no more than 300. Thus, the estimated efficiency gain from the contribution of the reduction of the amount of ray tracing is on the order of $G_r = 5430/300 \approx 18$.

2. The impulse response operator of parsimonious Kirchhoff migration is much smaller than that of conventional Kirchhoff migration. The extent of the impulse response of parsimonious migration is the first Fresnel zone of the local reflector surface around the estimated stationary reflection point, while in conventional migration it is a large isochronic surface. The latter is necessary since there isn't any information on where the exact location of stationary reflection point is, so the image is built up by constructive interference between adjacent trace contributions. In parsimonious migration, the reflector orientations are implicit in the ray parameter data and are made explicit by the ray tracing. We can estimate the efficiency contribution of the shrinking of the impulse response as

follows. For the salt model, the dominant frequency is f = 15 Hz, and if the average velocity v = 2.2 km/s, then, a typical wave length is λ = 0.147 km. If the average one-way ray length is s = 1.5 km, then we have the average radius of the first Fresnel zone at the local reflector surface (Yilmaz, 2001) as

$$r = \sqrt{(s\lambda/2)} = 0.332 \text{ (km)} \quad . \tag{3}$$

The area contained within the first Fresnel zone is $A_p = \pi r^2 = 0.346$ km^2. On the other hand, the area of the impulse response of conventional Kirchhoff migration is (Weast and Selby, 1967)

$$A_c = 2\pi z^2(1 - \sin\theta) \quad , \tag{4}$$

where z is the depth, and θ is the maximum dip. If z = 1.5 km and θ = 45°, then $A_c = 4.14$ km^2. Thus, the efficiency gain from the contraction of the impulse response operator is $G_i = A_c/A_P = 4.14/0.346 \approx 11$.

3. The input seismic data are decimated by the application of the amplitude threshold cut-off in parsimonious migration. The selection of the amplitude threshold depends on the quality of the input data and usually is determined by "trial and error". For our synthetic data for the salt model, when a threshold value 0.01 is used, the decimated data is about 0.1 of the original input data. Thus, the efficiency contribution due to the compression of input data is $G_c = 10$.

The composite efficiency gain from the above three factors is $G_t = G_c \times (G_r + G_i)$. Accurate estimation of the efficiency gains of parsimonious migration is very complicated and is both impossible and unnecessary. This example gives a representative $G_t = 10 \times (18 + 11) = 290$; the actual efficiency gain for the example (the salt model) from the computation times is $\sim$ 230 (Table 1), which is the same order of magnitude. If the ray parameter file structure is reorganized by grouping p-values at the same receiver location (see the Methodology section), an additional efficiency gain is obtained.

Parallel computation will also speed up parsimonious migration.The parallelization of ray parameter estimation step in parsimonious migration can be implemented by sorting the input seismic data into common-source gathers. Different common-source gathers can be read into different processors for the estimation of ray parameters of the traces in the common-source gathers. The parallelization of the migration step is easy: simply dividing the input data into blocks (without overlap between blocks), and each block can be migrated separately by a processor. The final migrated image is obtained by summing over all the partial migration outputs over all the processors used.

Parsimonious migration can also be applied to imaging of vertical seismic profile (VSP) data sets with only a small modification. The additional information needed is the velocity in the well where the geophones are placed. The well sonic log will provide the velocity information.

CONCLUSIONS

A very-fast implementation of input-based 3D prestack Kirchhoff depth migration has been illustrated. The new parsimonious Kirchhoff depth migration is extremely fast compared to conventional Kirchhoff migration because of the use of the ray parameter information estimated from the input seismic data and the applications of fast ray tracing, data decimation, and image aperture optimization. There is no inherent dip limitation, traveltime table calculation is obviated, and the time image condition is computed on-the-fly. The parsimonious migration has proved to be runnable on workstations (not only on supercomputers and processor clusters) for the two synthetic examples in this paper and is expected to be applicable to 3D field data sets.

The structural information of subsurface horizons obtained by parsimonious Kirchhoff migration is comparable to (and occasionally even better than) that obtained by conventional Kirchhoff migration. The parsimonious migrated images are cleaner than those obtained by conventional Kirchhoff migration, but are slightly less coherent. The amplitude information in the migrated images obtained by the current implementation of parsimonious migration is not correctly preserved and will be a future research topic. A more accurate final migration image can be obtained by using other (more complete and correspondingly more expensive) migration algorithms if desired.

The most obvious potential applications of parsimonious migration are as a component of low cost 3D iterative migration velocity analysis and to perform real-time migration imaging to get a fast first look at the structure for quality control in the field.

ACKNOWLEDGMENTS

The research leading to this paper was supported by the Sponsors of the UT-Dallas Geophysical Consortium and by the Texas Advanced Research Program under grant 009741-0021-2007. This paper is Contribution No. 1186 from the Department of Geosciences at the University of Texas at Dallas.

REFERENCES

Agnihotri, Y. and McMechan, G.A., 2007. Parsimonious migration of 3-C 3D VSP data. Geophysics, 72: S205-S213.

Aminzadeh, F., Brac, J. and Kunz, T., 1997. 3-D salt and overthrust models. SEG/EAGE 3-D modeling series No. 1. SEG, Tulsa, OK.

Červený, V., Molotkov, I.A. and Pšenćik, I., 1977. Ray method in seismology. Universita Karlova, Prague.

Coffin, M.F., Eldholm, O., Stoffa, P.L. and Dustin Jr., J.A., 1998. Looking ahead to the future of marine reflection seismology. EOS Trans., 79: 614-615.

Cordsen, A., Galbraith, M. and Peirce, J., 2000. Planning Land 3-D Seismic Surveys. SEG, Tulsa, OK.

Epili, D. and McMechan, G.A., 1996. Implementation of 3-D prestack Kirchhoff migration, with application to data from the Ouachita frontal thrust zone. Geophysics, 61: 1400-1411.

Fei, W. and McMechan, G.A., 2006a. Common reflection-point based seismic migration velocity analysis. Geophysics, 71: U21-U28.

Fei, W. and McMechan, G.A., 2006b. 3-D common reflection point based seismic migration velocity analysis. Geophysics, 71: S161-S167.

Fornberg, B., 1988. Generation of finite difference formulas on arbitrarily spaced grids. Mathemat. Computat., 51: 699-706.

Hua, B.-L., 2002. Parsimonious Kirchhoff depth migration. Ph.D. dissertation, Univ. of Texas, Dallas.

Hua, B.-L. and McMechan, G.A., 1999. Parsimonious Kirchhoff depth migration. Expanded Abstr., 69th Ann. Internat. SEG Mtg., Houston: 1382-1385.

Hua B.-L. and McMechan, G.A., 2001. Parsimonious 2-D poststack Kirchhoff depth migration. Geophysics, 66: 1497-1503.

Hua, B.-L. and McMechan, G.A., 2003. Parsimonious 2-D prestack Kirchhoff depth migration. Geophysics, 68: 1043-1051.

Hua, B.-L. and McMechan, G.A., 2005. Parsimonious 3-D poststack Kirchhoff depth migration. Geophys. Prosp., 53: 507-522.

Petroleum Geo-Services, 2008. Ramform. http://www.pgs.com/Geophysical/Services/Marine/Acquisition/Streamers_Seismic/Resources/Ramform/. Last accessed September 9, 2008.

Press, W.H., Teukolsky, S.A., Vettering, W.T. and Flannery, B.P., 1992. Numerical Recipes in C. Cambridge University Press, Cambridge.

Ratcliff, D.W., Gray, S.H. and Whitmore Jr., N,D., 1992. Seismic imaging of salt structures in The Gulf of Mexico. The Leading Edge, 11: 15-31.

Ratcliff, D.W., Jacewitz, C.A. and Gray, S.H., 1994. Subsalt imaging via target-oriented 3-D prestack depth migration. The Leading Edge, 13: 163-170.

Sheriff, R.E. and Geldart, L.P., 1982. Exploration Seismology. History, theory, and data acquisition. Cambridge University Press, Cambridge.

Um, J. and Thurber, C., 1987. A fast algorithm for two-point seismic ray tracing. Bull. Seismol. Soc. Am., 77: 972-986.

Weast, R.C. and Selby, S.M., 1967. Handbook of tables for mathematics. The Chemical Rubber Company.

Yilmaz, Ö., 2001. Seismic Data Analysis. SEG, Tulsa, OK.